

An investigation about the structures, thermodynamics and kinetics of the formic acid involved molecular clusters

Rui Zhang^a, Shuai Jiang^b, Yi-Rong Liu^b, Hui Wen^c, Ya-Juan Feng^b, Teng Huang^c, Wei Huang^{b,c,*}

^a School of Electronics and Information Engineering, Anhui Jianzhu University, Hefei, Anhui 230601, China

^b School of Information Science and Technology, University of Science and Technology of China, Hefei, Anhui 230026, China

^c Laboratory of Atmospheric Physico-Chemistry, Anhui Institute of Optics & Fine Mechanics, Chinese Academy of Sciences, Hefei, Anhui 230031, China

ARTICLE INFO

Article history:

Received 28 October 2017

In final form 25 March 2018

Available online 2 April 2018

ABSTRACT

Despite the very important role of atmospheric aerosol nucleation in climate change and air quality, the detailed aerosol nucleation mechanism is still unclear. Here we investigated the formic acid (FA) involved multicomponent nucleation molecular clusters including sulfuric acid (SA), dimethylamine (DMA) and water (W) through a quantum chemical method. The thermodynamics and kinetics analysis was based on the global minima given by Basin-Hopping (BH) algorithm coupled with Density Functional Theory (DFT) and subsequent benchmarked calculations. Then the interaction analysis based on ElectroStatic Potential (ESP), Topological and Atomic Charges analysis was made to characterize the binding features of the clusters. The results show that FA binds weakly with the other molecules in the cluster while W binds more weakly. Further kinetic analysis about the time evolution of the clusters show that even though the formic acid's weak interaction with other nucleation precursors, its effect on sulfuric acid dimer steady state concentration cannot be neglected due to its high concentration in the atmosphere.

© 2018 Published by Elsevier B.V.

1. Introduction

Atmosphere new particle formation has attracted lots of research for decades as they can influence the radiative forcing, climate change and human health significantly. New particle formation could be regarded as two distinct stages: nucleation and subsequent growth [1]. Mostly, the free energy barrier needs to be overcome for nucleation while the Kelvin barrier needs to be surmounted for growth [2–4]. According to Intergovernmental Panel on Climate Change (IPCC) 2013, the aerosol effects (direct & indirect) on climate change have been the largest uncertainty. Recent simulation studies [5–7] indicate that aerosol nucleation appears to dominate the total particle number concentration in many parts of the troposphere. However, the detailed aerosol nucleation mechanism is still mysterious even though many advances have been achieved in the recent years [8–13].

In 2007, Kurtén et al. [14] and Nadykto et al. [15] independently reviewed the advances obtained at that time for aerosol nucleation molecular clusters studies and pointed out the significance of

applying quantum chemistry into atmospheric aerosol nucleation area. From then on, till today, a large amount of quantum chemical calculations papers have been published focusing on various systems including sulfuric acid, ammonia [16], amines [17], organic acid [18–21] and organics oxidation products [22], especially focusing on their thermodynamics. Very recently, the kinetic studies about them have got lots of attention due to their excellent agreement between theoretical values and the experimental ones [23]. The kinetics studies could be tracked back to the 90's, however, the recent advances derived from the coupling between quantum chemistry based thermodynamic data and the kinetic birth-death equations [24].

In this study, one of the most popular organic acid in the atmosphere, formic acid (FA) interacting with the other common aerosol nucleation precursors including sulfuric acid (SA), dimethylamine (DMA) and water (W) was investigated. First, the quantum chemical method was benchmarked. Then after obtaining the global minima, their binding features were given with the aid of ElectroStatic Potential (ESP) analysis. Then the interaction analysis was made based on the analysis of topology and atomic charges. Finally, the thermodynamics and kinetics were analyzed to investigate the relation between Gibbs free energy change and evaporation rates as well as the effect of formic acid on the steady state concentration of sulfuric acid dimer.

* Corresponding author at: School of Information Science and Technology, University of Science and Technology of China, Hefei, Anhui 230026, China.

E-mail address: huangwei6@ustc.edu.cn (W. Huang).

2. Methodology

2.1. Global minima search: Basin-Hopping (BH) algorithm coupled with Density Functional Theory (DFT)

The global minima of $(\text{FA})_m(\text{SA})_n(\text{DMA})_p$ ($m = 0-2$, $n = 0-2$, $p = 0-2$), $(\text{FA})_1(\text{W})_1$ and $(\text{FA})_1(\text{SA})_1(\text{DMA})_1(\text{W})_n$ ($n = 1-3$) were searched by BH algorithm coupled with DFT implemented in Dmol³ [25] except that the structures of $(\text{SA})_1(\text{W})_1$ and $(\text{SA})_2$ were from the literature [34] calculated under the same combination of method and basis set with the same accuracy. In previous studies, this BH algorithm coupled with DFT method has been successfully applied to atmospheric relevant molecular clusters [26–29]. The number of BH searches ranged from 2 to 5 according to the cluster size. Every search was performed with 1000 Monte Carlo (MC) steps at 2000 K with randomly generated initial structures. The temperature was a crucial parameter in BH, which should be chosen carefully because it affected the tradeoff between the acceptance ratio and the sampling efficiency. At each MC step, all of the molecules were translated and rotated, and the maximum translational and rotational displacements were 2 Å and $\pi/2$, respectively. To prevent the divergence of the clusters, we compiled a function to check whether the intermolecular distances exceeded the range defined after the structure perturbation caused by the MC sampling. After each MC step, this function automatically determined whether the molecule moved more than 5 Å, which could cause the optimization to fail. If a large divergence occurred, then this function automatically moved the molecules closer together. The atoms in different molecules were not permitted to be closer than 2 Å to prevent the self-consistent field (SCF) calculation from failing to converge.

In Dmol³ [25], there were two steps in the optimization procedure: the first optimization step was at the PW91/DND level, and the second optimization step was at the PW91/DNP level. Next, these twice-optimized structures were optimized again using the Gaussian09 suite of programs [30] at the level of PW91PW91/6-311++G(3df,3pd). The default convergence criteria were defined in the Gaussian09 suite of programs [30]. Harmonic vibrational frequency analysis was performed to verify that no imaginary frequencies were present and consequently, the structure of interest represented a local or a global minimum on the potential energy surface.

2.2. Thermodynamics calculations: benchmark work for quantum chemistry method

One of the most important thermodynamic parameter for the aerosol nucleation molecular clusters is the Gibbs free energy change, ΔG . To obtain this, the method and basis set combination must be chosen wisely.

The Pople basis set 6-311++G(3df,3pd) is sufficient to produce converged structures, and the aug-cc-pV(T + d)Z basis set is generally not an improvement in nucleation clusters [31]. Based on several recent benchmark studies about nucleation clusters, we chose the most accurate density functionals (M06-2X, PW91PW91, ω B97X-D) in geometry optimization and subsequent frequency calculations procedure to obtain the Gibbs free energy change for the comparison between each other to confirm their accuracy and consistency. For comparison, B3LYP was added, too. This strategy was very similar to that in the recently published article about pinic acid binding with sulfuric acid [32] except with B3LYP added in this work. From Table 1, we could conclude that M06-2X, PW91PW91, ω B97X-D have showed very good consistency within 0.82 kcal/mol difference while B3LYP significantly overestimate the Gibbs free energy change of all the three reactions. So based

on these benchmark results and the largest popularity of PW91PW91 functional in estimating the structures, vibrational frequencies and thermodynamics of nucleation clusters, we finally utilized PW91PW91/6-311++G(3df,3pd) to make the final geometry optimization and frequency calculations.

2.3. Kinetic calculations: collision rate constant and evaporation rate

The Gibbs free energy change mentioned above is an important parameter to indicate whether the clustering process is spontaneous or not. To further check the stability of molecular clusters, the properties including the mass and radius of clusters are fed into the collision rate constant calculations. In addition, the evaporation rate would be derived from the detailed balance with the collision rate constant and the Gibbs free energy change involved. The collision rate constant is normally calculated from the gas kinetic theory [33]:

$$\beta_{ij} = \left(\frac{3}{4\pi}\right)^{1/6} \left(\frac{6k_bT}{m_i} + \frac{6k_bT}{m_j}\right)^{1/2} (V_i^{1/3} + V_j^{1/3})^2 \quad (1)$$

$$\gamma_{(i+j) \rightarrow i} = \beta_{ij} \frac{P_0}{k_bT} \exp\left(\frac{\Delta G_{i+j} - \Delta G_i - \Delta G_j}{k_bT}\right) \quad (2)$$

where β and γ is collision rate constant (unit: $\text{m}^3 \text{s}^{-1}$) and evaporate rate (unit: s^{-1}) respectively, i and j is the collision cluster, k_b is Boltzmann constant (unit: J/K), T is temperature (unit: Kelvin), m is mass (unit: kg), V is volume (unit: m^3), P_0 is pressure in STP (standard temperature and pressure, $T = 298.15 \text{ K}$ and $P = 1 \text{ atm}$) conditions, ΔG is the Gibbs free energy change derived from quantum chemistry calculations.

The birth-death equations represent the time evolution of cluster with each size including the collision and evaporation processes [24]:

$$\frac{dc_i}{dt} = \frac{1}{2} \sum_{j < i} \beta_{j,(i-j)} c_j c_{i-j} + \sum_j \gamma_{(i+j) \rightarrow i} c_{i+j} - \sum_j \beta_{ij} c_i c_j - \frac{1}{2} \sum_{j < i} \gamma_{i-j} c_i - \text{CoagS} \quad (3)$$

where c represents concentration (m^{-3}), t is the simulation time (s), β , γ , i and j are the same symbols as those in Eqs. (1) and (2), CoagS is the coagulation sink (s^{-1}). The steady state is reached when the Ordinary Differential Equations (ODEs) are solved in convergence and the simulation time is long enough that the cluster concentration in each size changes no more.

3. Results and discussion

3.1. The global minima of the investigated clusters

Interesting binding features could be seen from the global minima of FA-involved clusters given in Fig. 1. For $(\text{FA})_1(\text{W})_1$ cluster, structures of FA and W both are planar, however, the cluster is not planar with a dihedral angle of 114 degree. Moreover, FA forms a cycle structure with SA with hydrogen atom in the hydroxyl in each molecule being the proton donor. Since there is only one amino group in DMA, the FA naturally becomes the proton donor molecule, but the stronger acidity of SA comparing with that of FA, in $(\text{FA})_1(\text{SA})_1(\text{DMA})_1$ cluster, SA turns to be the proton donor with binding with DMA directly and FA binds with SA and DMA. However, in the hydrate cluster, FA only binds with SA while W and SA bind with DMA directly. And since all the strong binding groups including hydroxyl group in acid and amino group in DMA are occupied in $(\text{FA})_1(\text{SA})_1(\text{DMA})_1(\text{W})_1$, few room left for the binding of more water molecules, resulting in the very weak Gibbs free energy change of $(\text{FA})_1(\text{SA})_1(\text{DMA})_1(\text{W})_2$ and

Table 1
The Gibbs free energy change (kcal/mol) of the three reactions calculated based on the functional of M06-2X, PW91PW91, ω B97X-D and B3LYP with the same basis set, 6-311++G(3df,3pd).

	M06-2X	PW91PW91	ω B97X-D	B3LYP
$\text{FA} + \text{W} \rightleftharpoons (\text{FA})_1(\text{W})_1$	-0.56	-0.44	0.09	1.41
$\text{FA} + \text{SA} \rightleftharpoons (\text{FA})_1(\text{SA})_1$	-7.35	-6.93	-6.53	-4.62
$\text{FA} + \text{DMA} \rightleftharpoons (\text{FA})_1(\text{DMA})_1$	-3.35	-2.77	-2.77	-0.22

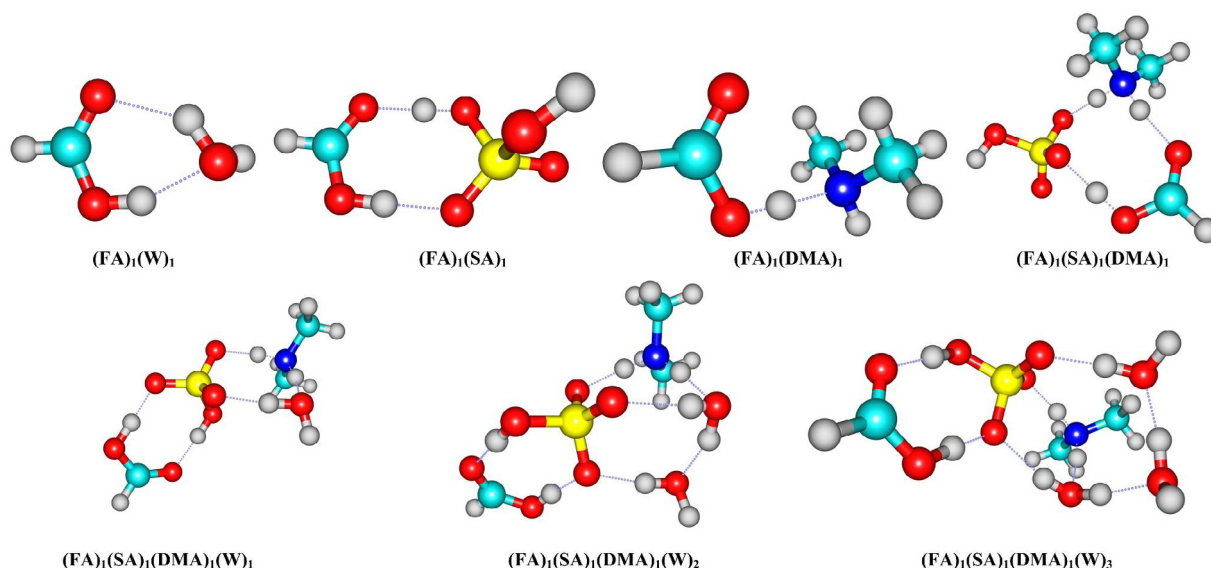


Fig. 1. The global minima geometries for FA involved molecular clusters calculated at the theory level of PW91PW91/6-311++G(3df,3pd), where FA, SA, DMA and W is short for formic acid, sulfuric acid, dimethylamine and water, respectively. The subscript in each cluster name refers to the corresponding molecule number in the cluster.

$(\text{FA})_1(\text{SA})_1(\text{DMA})_1(\text{W})_3$ changing from $(\text{FA})_1(\text{SA})_1(\text{DMA})_1(\text{W})_1$ as shown in Fig. 3. Proton transfer rarely happens in FA involved clusters even though the elongated O–H covalent bond could be seen in $(\text{FA})_1(\text{SA})_1(\text{DMA})_1$ with it changing from 0.979 Å in FA monomer to 1.035 Å in this cluster.

3.2. ESP analysis

ESP on van der Waals (vdW) surface has been applied on the study of the reactivity of Aristolochic acid [35]. For the clustering processes, the binding site could be analyzed by combing the featured group and ESP. The site possessing more negative ESP has the stronger ability to attract proton while those with more positive ESP tend to provide proton if the proton is available. Here we take the $(\text{FA})_1(\text{SA})_1$ cluster for instance since its binding ability is the strongest among FA involved dimers. As can be seen in Fig. 2, oxygen atom with the most negative potential (the reddest region) in FA molecule attracts the hydrogen atom with the most positive

potential (the bluest region) in SA molecule. On the other hand, oxygen atom with the most negative potential (the reddest region) in SA molecule attracts the hydrogen atom with the most positive potential (the bluest region) in FA molecule. Finally, two hydrogen bonds form to make the dimer energy as low as possible.

3.3. Topological analysis

The bond critical points (BCPs) shown in the topological graphs indicate the existence of intermolecular interactions in the complex. The line of maximum density passing through the BCP and linking the nuclei of the two atoms is then called a bond path. The values of the electron density ρ and its Laplacian $\nabla^2\rho$, as well as the electronic kinetic, potential and total energies ($G(r)$, $V(r)$ and $K(r)$, respectively) at the BCP can be used to characterize the nature of the bonding interaction [36].

The values of $\nabla^2\rho$ and $K(r)$ indicate the nature of the interaction. A negative value of $\nabla^2\rho$ indicates that there is a shared inter-

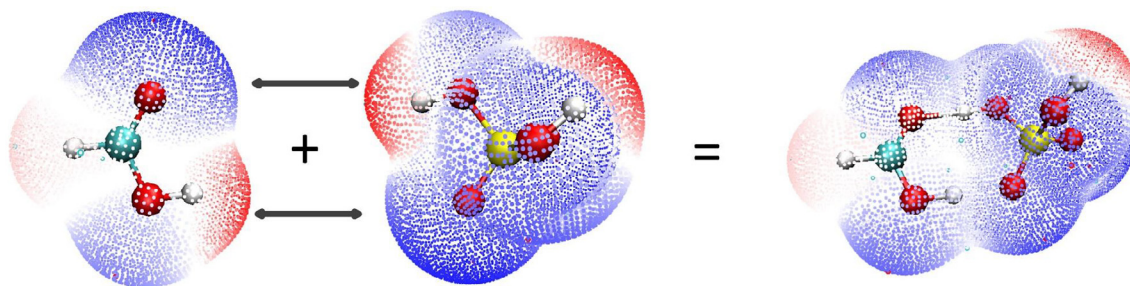


Fig. 2. The ElectroStaticPotential (ESP) analysis of formic acid, sulfuric acid and $(\text{FA})_1(\text{SA})_1$ cluster where FA represents formic acid while SA represents sulfuric acid.

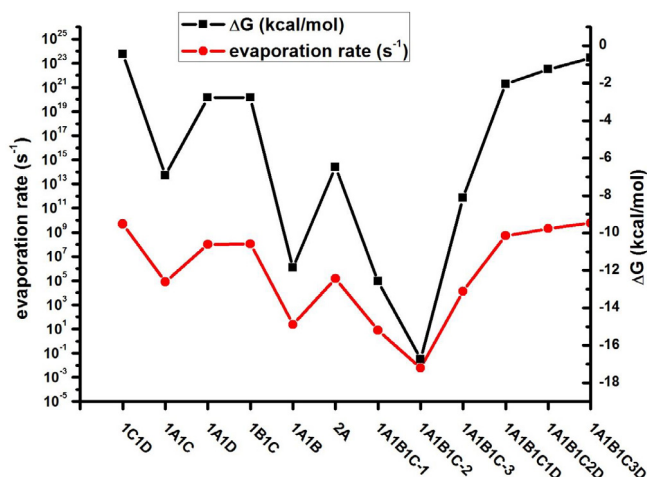


Fig. 3. The ΔG (kcal/mol) and evaporation rate (s^{-1}) for all the investigated clusters, where FA, SA, DMA and W is short for formic acid, sulfuric acid, dimethylamine and water, respectively and the sequence number is the same as that in Table 4.

action like in a covalent bond, whereas a positive value of $\nabla^2\rho$ indicates closed-shell system interactions, that is, ionic interactions, van der Waals forces, or hydrogen bonding [37]. On the other hand, if $\nabla^2\rho$ is positive but $K(r)$ is negative, then the interaction is partly covalent in nature [38,39]. Taking $-G(r)/V(r)$ as the balance between the positive value of $G(r)$ and the negative value of $V(r)$ may indicate the regions corresponding to covalent or noncovalent interactions. That is, if $-G(r)/V(r)$ is greater than 1, then the interaction is noncovalent. If the ratio is between 0.5 and 1, the interaction is partly covalent in nature, and when this ratio is less than 0.5, the interaction is a shared covalent interaction.

As shown in Table 2, for the BCPs of O4–H7...O5 in $(\text{FA})_1(\text{W})_1$ and C6–H11...O4 (please see Fig. S1 for the corresponding atom sequence number) as well as C8–H14...O4 in $(\text{FA})_1(\text{DMA})_1$, the result that the values of $\nabla^2\rho$ and $K(r)$ are both positive and $-G(r)/V(r)$ is larger than 1 indicates that these binding display the characteristics of “close-shell” noncovalent interactions. Comparatively, for the BCPs of O3–H1...O6 in $(\text{FA})_1(\text{W})_1$, O9–H11...O4 as well as O3–H1...O7 in $(\text{FA})_1(\text{SA})_1$, O3–H1...N7 in $(\text{FA})_1(\text{DMA})_1$ and N9–H6...O4 as well as N9–H14...O3 in $(\text{SA})_1(\text{DMA})_1$, $\nabla^2\rho > 0$, $K(r) < 0$ and $-G(r)/V(r)$ is between 0.5 and 1, so these interaction are partly covalent in nature.

For hydrogen bonded complexes, Koch and Popelier proposed eight topological criteria based on the theory of atoms in molecules to characterize the types of hydrogen bonds [40]. The closed-shell interactions (e.g., ionic bonds, hydrogen bonds, and van der Waals interactions) correspond to a positive value of Laplacian of charge density at BCP, whereas for covalent bonds the Laplacian has a neg-

ative value. The strength of the hydrogen bonds correlates with the charge density and, in general, the larger the charge density, the stronger the hydrogen bond. Two quantitative criteria have been suggested to characterize the strength of a hydrogen bond: the charge density and its Laplacian, in the range of 0.002–0.035 and 0.024–0.139 au, respectively [41].

In Table 2, it can be seen that most of charge density for the bonds in the table exceed 0.035 except two bonds in $(\text{FA})_1(\text{DMA})_1$ and one bond in $(\text{FA})_1(\text{W})_1$ while for Laplacian, all the three bonds in $(\text{FA})_1(\text{DMA})_1$ give very low values and none exceeds the upper limit but bonds in $(\text{SA})_1(\text{DMA})_1$ show relatively higher values. So it agrees with the Gibbs free energy change order approximately: $(\text{SA})_1(\text{DMA})_1$ binds with a strong hydrogen bond, $(\text{FA})_1(\text{SA})_1$ binds with a moderate hydrogen bond and $(\text{FA})_1(\text{W})_1$ and $(\text{FA})_1(\text{DMA})_1$ binds weakly.

3.4. Atomic charges analysis

Atomic charges model is a very simple and intuitive one for describing charge distribution and can be used to analyze the strength of electrostatic interaction between different sites [42]. For molecular cluster composing of acid and base here, atomic charges analysis is especially suitable since normally proton transfer would happen with charge transferring as well.

Among the various ways to obtain atomic charges, Hirshfeld method is most popular, which is based on deformation density partition. However, the disadvantages of Hirshfeld population are the always too small charges and the poor reproducibility of observable quantities, such as molecular dipole moment and ESP. The reason is Hirshfeld population completely ignores atomic dipole moments. In recently proposed ADCH method [43], Hirshfeld charges are corrected by expanding atomic dipole moments to correction charges placed at neighbour atoms. ADCH atomic charges are very reasonable in chemical sense, molecular dipole moment is exactly reproduced, the reproducibility of ESP is close to the atomic charges from fitting ESP. Owing to its many advantages, ADCH is a highly recommended atomic charges model [42]. So here we use ADCH to obtain atomic charges of molecule in clusters.

It is expected that the acidic molecule shows negative atomic charges values while the basic one shows positive values, so from ADCH atomic charges of the investigated clusters in Table 3, FA acidity is weaker than that of SA given by the atomic charges of $(\text{FA})_1(\text{SA})_1$. However, even though FA binds more closely with SA than with DMA derived from Table 1, the absolute value of atomic charges of $(\text{FA})_1(\text{SA})_1$ is smaller than $(\text{FA})_1(\text{DMA})_1$ probably due to one acid counteracting another acid in this case. Besides, deriving from atomic charges of hydration clusters, the influence of water molecule on cluster is negligible.

Table 2

The bond lengths (Å) and topological properties (a.u.) at Bond Critical Points (BCPs) for the global minima of the investigated molecular clusters (please see Fig. S1 for the corresponding atom sequence number).

Complex	Bond notation	Bond length	$\rho(10^{-2})$	$\nabla^2\rho(10^{-2})$	$G(r)(10^{-2})$	$K(r)(10^{-2})$	$V(r)(10^{-2})$	$-G(r)/V(r)$
$(\text{FA})_1(\text{W})_1$	O3–H1...O6	1.713	4.71	10.57	3.51	−0.87	−4.37	0.80
	O4–H7...O5	1.921	2.94	9.16	2.28	0.01	−2.27	1.00
$(\text{FA})_1(\text{SA})_1$	O9–H11...O4	1.503	7.73	8.62	5.21	−3.06	−8.27	0.63
	O3–H1...O7	1.632	5.32	10.62	3.99	−1.34	−5.33	0.75
$(\text{FA})_1(\text{DMA})_1$	O3–H1...N7	1.053	7.60	3.10	4.00	−3.23	−7.24	0.55
	C6–H11...O4	2.680	0.71	2.17	0.47	0.07	−0.40	1.18
	C8–H14...O4	2.681	0.71	2.17	0.47	0.07	−0.40	1.18
$(\text{SA})_1(\text{DMA})_1$	N9–H6...O4	1.626	5.40	12.02	4.11	−1.10	−5.21	0.79
	N9–H14...O3	1.672	6.04	11.76	4.49	−1.55	−6.03	0.74

Table 3
The ADCH atomic charges for all the investigated clusters.

Complex	Fragment			
(FA) ₁ (W) ₁	−0.11		0.11	
(FA) ₁ (SA) ₁	0.04		−0.04	
(FA) ₁ (DMA) ₁	−0.21		0.21	
(SA) ₁ (DMA) ₁	−0.48		0.48	
(FA) ₁ (SA) ₁ (DMA) ₁	−0.04	−0.42		0.46
(FA) ₁ (SA) ₁ (DMA) ₁ (W) ₁	−0.07	−0.41	0.46	0.03
(FA) ₁ (SA) ₁ (DMA) ₁ (W) ₂	−0.07	−0.38	0.45	0.00
(FA) ₁ (SA) ₁ (DMA) ₁ (W) ₃	−0.07	−0.35	0.43	−0.01

Notation: The order in the “Fragment” column is the same as that in the cluster formula, for example, the first box in the “Fragment” column for complex (FA)₁(W)₁ represents FA while the second one represents W. And for the hydration clusters, in order to investigate the hydration effect, the water molecules in the complex were put into one fragment.

3.5. Thermodynamics and kinetics: ΔG , collision rate constant and evaporation rate analysis

From the relation between evaporation rate and ΔG shown in Fig. 3, on the whole, all the clustering processes considering here happen spontaneously in STP. From the total evaporation rate given in Table 4, the most stable cluster is (SA)₁(DMA)₁ while the most unstable cluster is (FA)₁(SA)₁(DMA)₁(W)₃. It has to be mentioned here that not all the clustering processes are considered here (e.g. the non-monomer collision and evaporation processes are neglected), so the evaporation rate here for clusters larger than dimer is the lower bound for the actual evaporation rate.

From Table 4, we could see the different affinity of FA, SA, DMA and H₂O for the various reactions there. For FA affinity, the affinity order is: SA > DMA > H₂O, which is quite surprising because comparing with DMA, the acid-acid reaction is more feasible surprisingly.

3.6. The effect of formic acid on the sulfuric acid dimer steady state concentration in STP

Here the kinetic analysis focused on the effect of formic acid on the total cluster concentration of SA₂(DMA)_m ($m = 0-2$) and (FA)_n(SA)₂ ($n = 1-2$) which was thought to be the sulfuric acid dimer concentration, [SA Dimer] (in the following part, “[]” would be regarded as the symbol of concentration). In addition, (FA)_m(SA)_n(DMA)_p ($m = 0-2$, $n = 0-2$, $p = 0-2$) were include for kinetic simulation while (FA)₁(W)₁ and (FA)₁(SA)₁(DMA)₁(W)_n ($n = 1-3$) were excluded because the involvement of water molecules was unnecessary for considering the effect of formic acid on the steady state concentration of sulfuric acid dimer.

For the simulation of the ambient atmospheric conditions, Nanjing is chosen for instance since it is a good representative of polluted megacities in Yangtze River Delta (YRD) region of China. The initial SA concentration is set to be 2.0E+7 and 2.0E+9 cm^{−3}

to represent the low and high sulfuric acid concentration case respectively, considering campaign observation values conducted in Nanjing (Yu et al., 2016) while the initial DMA concentration is set to be 2 and 200 ppt to represent the low and high base concentration case respectively, according to the C2-amines concentration measured from another field campaign conducted in Nanjing (Zheng et al., 2015). For the concentration of FA, since atmospheric observation of gas phase FA in Nanjing is scarce, here we use the average values in the urban sites of Japan and U.S. for reference, which is ranging from 0.2 to 20 ppb.

To test whether the steady state is reached within the given reaction time (here is 2000 s), cluster concentration calculated under longer time (3000 s) is provided for comparison and it turns out that 2000 s is long enough for reaching the steady state under the conditions considered here. The boundary condition is that if the cluster is equal or more than (SA)₃(DMA)₃, it would be regarded to be stable enough to be out of the simulation. CoagS is set to be 2.2E−2 s^{−1} according to the field observation conducted in Nanjing. The total concentration of (SA)₁(FA)_m ($m = 0-2$) and (SA)₁(DMA)_m ($m = 1-2$) is kept to be constant during the time evolution considering that the molecule or cluster binding with sulfuric acid monomer would evaporate in the chemical ionization mass spectrometer (CIMS) in the field observation.

In Fig. 4, when the initial acid or base concentration was increased like from Fig. 4(a) to Fig. 4(b) or Fig. 4(a) to Fig. 4(c) while the initial formic acid kept constant, [SA Dimer] increased accordingly. However, the effect of formic acid on [SA Dimer] showed non-monotonic behavior if we look at the drop percent of [SA Dimer] when [FA] was increased from zero to 20 ppb. In addition, this effect decreased with the increase of [FA] as we could see the decrease of the curve slope. The highest drop percent was 90.55% while the lowest drop percent was 31.91%, indicating the non-ignorable role of formic acid for the aerosol nucleation cluster population. This showed the importance of kinetic simulation so that the competition between weak binding effect and high

Table 4
The collision rate constant and the evaporation rate of the clustering processes.

No.#	Reactions	Collision rate constant (m ³ s ^{−1})	Total evaporation rate (s ^{−1})
1	FA + W ⇌ (FA) ₁ (W) ₁	4.23e−16	4.98e+09
2	FA + SA ⇌ (FA) ₁ (SA) ₁	3.86e−16	7.88e+04
3	SA + W ⇌ (SA) ₁ (W) ₁	4.46e−16	1.02e+08
4	FA + DMA ⇌ (FA) ₁ (DMA) ₁	4.89e−16	1.12e+08
5	SA + DMA ⇌ (SA) ₁ (DMA) ₁	4.69e−16	2.33e+01
6	SA + SA ⇌ (SA) ₂	3.46e−16	1.52e + 05
7	(FA) ₁ (SA) ₁ + DMA ⇌ (FA) ₁ (SA) ₁ (DMA) ₁	5.32e−16	1.33e+04
8	(FA) ₁ (DMA) ₁ + SA ⇌ (FA) ₁ (SA) ₁ (DMA) ₁	4.45e−16	
9	(SA) ₁ (DMA) ₁ + FA ⇌ (FA) ₁ (SA) ₁ (DMA) ₁	4.96e−16	
10	(FA) ₁ (SA) ₁ (DMA) ₁ + W ⇌ (FA) ₁ (SA) ₁ (DMA) ₁ (W) ₁	6.77e−16	5.35E+08
11	(FA) ₁ (SA) ₁ (DMA) ₁ (W) ₁ + W ⇌ (FA) ₁ (SA) ₁ (DMA) ₁ (W) ₂	7.08e−16	2.02E+09
12	(FA) ₁ (SA) ₁ (DMA) ₁ (W) ₁ + W ⇌ (FA) ₁ (SA) ₁ (DMA) ₁ (W) ₃	7.38e−16	5.83E+09

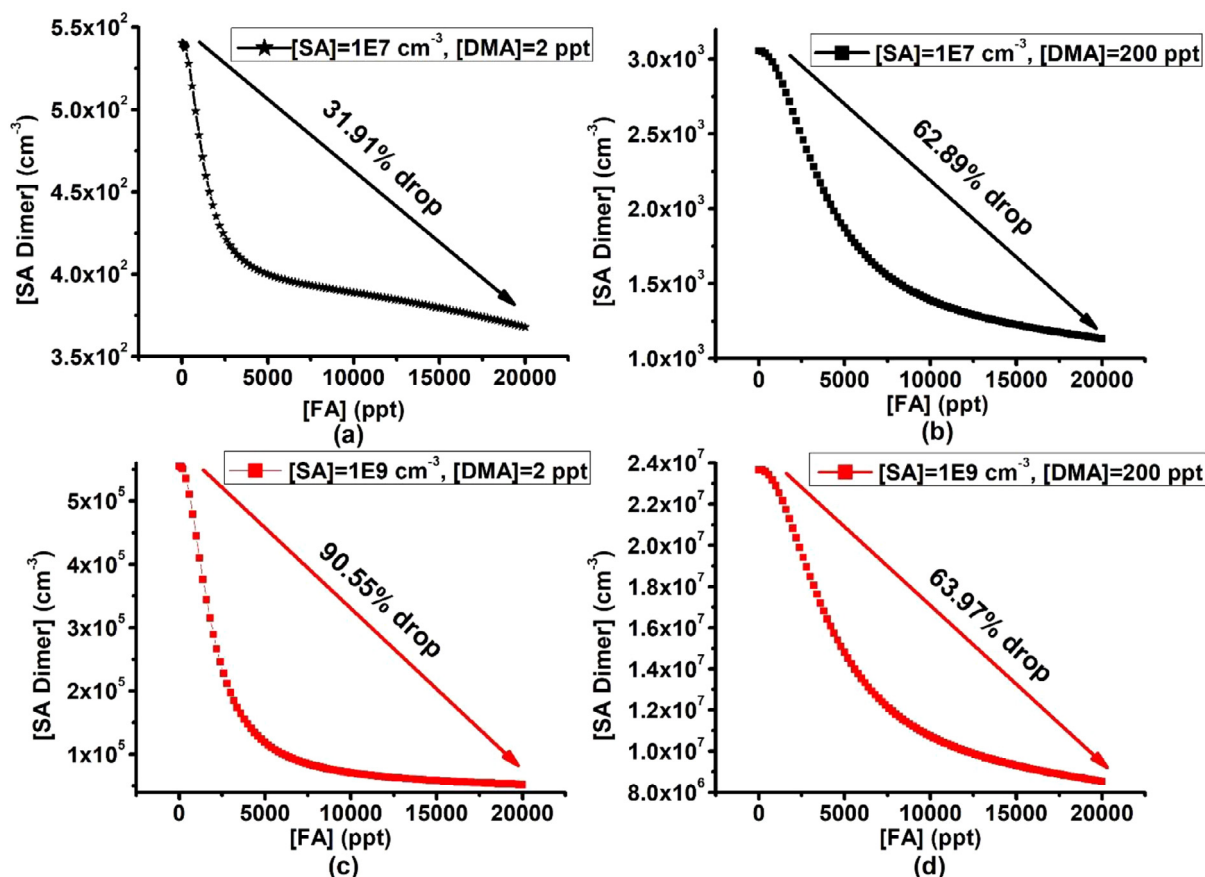


Fig. 4. Sulfuric acid dimer concentration ($[SA \text{ Dimer}]$ in cm^{-3}) dependence on the change of formic acid monomer concentration ($[FA]$ in ppt, from 0 ppt to 20 ppt) under different initial sulfuric acid monomer concentration ($[SA]$ in cm^{-3}) and dimethylamine monomer concentration ($[DMA]$ in ppt) at the steady state: (a) $[SA] = 1\text{E}7 \text{ cm}^{-3}$, $[DMA] = 2 \text{ ppt}$; (b) $[SA] = 1\text{E}7 \text{ cm}^{-3}$, $[DMA] = 200 \text{ ppt}$; (c) $[SA] = 1\text{E}9 \text{ cm}^{-3}$, $[DMA] = 2 \text{ ppt}$; (d) $[SA] = 1\text{E}9 \text{ cm}^{-3}$, $[DMA] = 200 \text{ ppt}$.

concentration effect on the cluster population like formic acid in this case would be characterized clearly.

4. Conclusions

In the view of method verification, PW91PW91, M06-2X and ω B97X-D could give a similar description of thermodynamics of FA involved clusters while B3LYP overestimates that. In addition, ESP provides us a powerful tool to confirm the reaction/binding site in molecular clusters.

For the atmospheric implication, the thermodynamic analysis of the investigated clusters indicates that FA could bind with SA/DMA at STP but significantly weaker than the interaction between SA and DMA, which is verified by topological and atomic charge analysis. The binding ability of water molecule in the investigated ternary clusters is very weak suggesting the less important role of hydration in these clusters. Even though the weak interaction between FA and SA/DMA, the steady state concentration of the potential critical cluster, $[SA \text{ Dimer}]$ could be significantly influenced by the introduction of FA, which signifies the complexity of multicomponent nucleation and necessity of taking more nucleation precursors into consideration.

Acknowledgments

This work was supported by the National Natural Science Foundation of China (Grant Nos. 21403244, 41775122, 21573241, 41605099, 41705097, 41705111, 41775112 and 41527808), the National Science Fund for Distinguished Young Scholars (Grant

No. 41725019), Key Research Program of Frontier Science, CAS (Grant No. QYZDB-SSW-DQC031), The Key Research Program of the Chinese Academy of Sciences (Grant No. ZDRW-ZS-2016-4-3-6) and the National Key Research and Development program (Grant Nos. 2016YFC0202203 and 2016YFC0203703).

Appendix A. Supplementary data

Supplementary data associated with this article can be found, in the online version, at <https://doi.org/10.1016/j.chemphys.2018.03.029>.

References

- [1] R. Zhang, A. Khalizov, L. Wang, M. Hu, W. Xu, *Chem. Rev.* 112 (2012) 1957.
- [2] C. Qiu, R. Zhang, *Phys. Chem. Chem. Phys.* 15 (2013) 5738.
- [3] L. Wang, A.F. Khalizov, J. Zheng, W. Xu, Y. Ma, V. Lal, R. Zhang, *Nat. Geosci.* 3 (2010) 238.
- [4] C. Qiu, L. Wang, V. Lal, A.F. Khalizov, R. Zhang, *Environ. Sci. Technol.* 45 (2011) 4748.
- [5] F. Yu, G. Luo, T.S. Bates, B. Anderson, A. Clarke, V. Kapustin, R.M. Yantosca, Y. Wang, S. Wu, *J. Geophys. Res.* 115 (2010) D17205.
- [6] F. Yu, G. Luo, *Atmos. Chem. Phys.* 9 (2009) 7691.
- [7] D. Spracklen, K. Carslaw, M. Kulmala, V.-M. Kerminen, G. Mann, S.-L. Sihto, *Atmos. Chem. Phys.* 6 (2006) 5631.
- [8] M. Kulmala, T. Petäjä, M. Ehn, J. Thornton, M. Sipilä, D. Worsnop, V.-M. Kerminen, *Annu. Rev. Phys. Chem.* 65 (2014) 21.
- [9] E.M. Dunne, H. Gordon, A. Kürten, J. Almeida, J. Duplissy, C. Williamson, I.K. Ortega, K.J. Pringle, A. Adamov, U. Baltensperger, *Science* 354 (2016) 1119.
- [10] J. Kirkby, J. Duplissy, K. Sengupta, C. Frege, H. Gordon, C. Williamson, M. Heinritzi, M. Simon, C. Yan, J. Almeida, *Nature* 533 (2016) 521.
- [11] M. Sipilä, N. Sarnela, T. Jokinen, H. Henschel, H. Junninen, J. Kontkanen, S. Richters, J. Kangasluoma, A. Franchin, O. Peräkylä, *Nature* 537 (2016) 532.

- [12] F. Bianchi, J. Tröstl, H. Junninen, C. Frege, S. Henne, C. Hoyle, U. Molteni, E. Herrmann, A. Adamov, N. Bukowiecki, *Science* 352 (2016) 1109.
- [13] J. Tröstl, W.K. Chuang, H. Gordon, M. Heinritzi, C. Yan, U. Molteni, L. Ahlm, C. Frege, F. Bianchi, R. Wagner, *Nature* 533 (2016) 527.
- [14] T. Kurtén, H. Vehkamäki, *Adv. Quantum Chem.* 55 (2008) 407.
- [15] A.B. Nadykto, A. Al Natsheh, F. Yu, K.V. Mikkelsen, J. Herb, *Adv. Quantum Chem.* 55 (2008) 449.
- [16] A. Nadykto, F. Yu, J. Herb, *Atmos. Chem. Phys.* 9 (2009) 4031.
- [17] T. Kurtén, V. Loukonen, H. Vehkamäki, M. Kulmala, *Atmos. Chem. Phys.* 8 (2008) 4095.
- [18] R. Zhang, I. Suh, J. Zhao, D. Zhang, E.C. Fortner, X. Tie, L.T. Molina, M.J. Molina, *Science* 304 (2004) 1487.
- [19] W. Xu, R. Zhang, *J. Phys. Chem. A* 116 (2012) 4539.
- [20] W. Xu, R. Zhang, *J. Chem. Phys.* 139 (2013) 064312.
- [21] J. Zhao, A. Khalizov, R. Zhang, R. McGraw, *J. Phys. Chem. A* 113 (2009) 680.
- [22] J. Elm, N. Myllys, N. Hyttinen, T. Kurtén, *J. Phys. Chem. A* 119 (2015) 8414.
- [23] J. Almeida, S. Schobesberger, A. Kürten, I.K. Ortega, O. Kupiainen-Määttä, A.P. Praplan, A. Adamov, A. Amorim, F. Bianchi, M. Breitenlechner, *Nature* 502 (2013) 359.
- [24] M. McGrath, T. Olenius, I. Ortega, V. Loukonen, P. Paasonen, T. Kurtén, M. Kulmala, H. Vehkamäki, *Atmos. Chem. Phys.* 12 (2012) 2345.
- [25] B. Delley, *J. Chem. Phys.* 92 (1990) 508.
- [26] J. Chen, S. Jiang, Y.-R. Liu, T. Huang, C.-Y. Wang, S.-K. Miao, Z.-Q. Wang, Y. Zhang, W. Huang, *RSC Adv.* 7 (2017) 6374.
- [27] S. Jiang, T. Huang, Y.-R. Liu, K.-M. Xu, Y. Zhang, Y.-Z. Lv, W. Huang, *Phys. Chem. Chem. Phys.* 16 (2014) 19241.
- [28] S. Jiang, Y.R. Liu, T. Huang, H. Wen, K.M. Xu, W.X. Zhao, W.J. Zhang, W. Huang, *J. Comput. Chem.* 35 (2014) 159.
- [29] S.-K. Miao, S. Jiang, J. Chen, Y. Ma, Y.-P. Zhu, Y. Wen, M.-M. Zhang, W. Huang, *RSC Adv.* 5 (2015) 48638.
- [30] M. Frisch, G. Trucks, H.B. Schlegel, G. Scuseria, M. Robb, J. Cheeseman, G. Scalmani, V. Barone, B. Mennucci, G. Petersson, in: *Gaussian 09, Revision A.02*, Gaussian, Inc., Wallingford, CT, 2009, p. 271.
- [31] J. Elm, M. Bilde, K.V. Mikkelsen, *J. Chem. Theory Comput.* 8 (2012) 2071.
- [32] J. Elm, T. Kurtén, M. Bilde, K.V. Mikkelsen, *J. Phys. Chem. A* 118 (2014) 7892.
- [33] S. Chapman, T.G. Cowling, *Cambridge university press*, 1970.
- [34] A.B. Nadykto, J. Herb, F. Yu, Y. Xu, *Chem. Phys. Lett.* 609 (2014) 42.
- [35] S. Manzetti, T. Lu, *J. Phys. Org. Chem.* 26 (2013) 473.
- [36] R.F. Bader, *J. Phys. Chem. A* 102 (1998) 7314.
- [37] R.F. Bader, *Wiley Online Library*, 1990.
- [38] D. Cremer, E. Kraka, *Angew. Chem. Int. Ed.* 23 (1984) 627.
- [39] R.G. Bone, R.F. Bader, *J. Phys. Chem.* 100 (1996) 10892.
- [40] U. Koch, P. Popelier, *J. Phys. Chem.* 99 (1995) 9747.
- [41] P. Gilli, V. Bertolasi, V. Ferretti, G. Gilli, *J. Am. Chem. Soc.* 116 (1994) 909.
- [42] T. Lu, F. Chen, *J. Comput. Chem.* 33 (2012) 580.
- [43] T. Lu, F. Chen, *J. Theor. Comput. Chem.* 11 (2012) 163.